Surface-Enhanced Resonance Raman Spectroscopy for the Rapid Detection of Cryptosporidium parvum and Giardia lamblia

ARTICLE *in* ENVIRONMENTAL SCIENCE AND TECHNOLOGY · MARCH 2009

Impact Factor: 5.33 · DOI: 10.1021/es801531t · Source: PubMed

Environ. Sci. Technol. **2009,** *43,* 1147–1152

Surface-Enhanced Resonance Raman Spectroscopy for the Rapid Detection of *Cryptosporidium parvum* and *Giardia lamblia*

KRISTA L. RULE AND PETER J. VIKESLAND*

Department of Civil and Environmental Engineering, Virginia Polytechnic Institute and State University, 418 Durham Hall, Blacksburg, Virginia 24060-0246

Received June 3, 2008. Revised manuscript received November 11, 2008. Accepted November 13, 2008.

A rapid surface-enhanced resonance Raman spectroscopy (SERRS) method has been developed for the detection of two waterborne pathogens, *Cryptosporidium parvum* and *Giardia lambia*. Raman labels were prepared by conjugating gold nanoparticles with commercial antibodies and dye molecules. After incubation with the immunogold labels, *C. parvum* oocysts and *G. lamblia* could easily be measured and differentiated by Raman spectroscopy. The immunogold signal intensities were optimized by testing several sizes of gold nanoparticles, four different commercially available dye molecules, and two Raman excitation wavelengths. Raman maps were collected across fixed and labeled *Cryptosporidium* oocysts and *Giardia* cysts, and the maps were used to determine which *C. parvum* and *G. lamblia* antibodies exhibited the best specificities and organism coverages. Ultimately, 40 nm gold nanoparticles were conjugated with rhodamine B isothiocyanate and malachite green isothiocyanate for the *C. parvum* and *G. lamblia* immunogold syntheses, respectively. *C. parvum* monoclonal IgM antibodies and *G. lamblia* monoclonal IgG1 antibodies resulted in the best immunogold coverage. The research presented here demonstrates the feasibility of utilizing SERRS labeling for sensitive multipathogen monitoring strategies.

Introduction

Despite major advances in water treatment, periodic outbreaks of waterborne disease continue to plague both developing and developed countries. In addition, human population growth and climate change are expected to lead to increases in the number of species and the concentrations of waterborne pathogens in surface water and groundwater. To minimize the chances for outbreaks, drinking water utilities monitor their finished waters for pathogens that survive treatment. Pathogen monitoring programs protect the public against naturally occurring pathogens and potential bioterrorist threats to drinking water supplies.

In the United States, finished drinking waters are monitored for total coliform, *Cryptosporidium parvum*, and *Giardia lamblia* (*1*). Coliform bacteria are a subset of Gram-negative bacteria that have historically been used as fecal surrogates in water monitoring. *C. parvum* and *G. lamblia* are protozoan pathogens that can cause gastrointestinal illnesses that are potentially deadly for immunocompromised individuals. During water treatment, *C. parvum* and *G. lamblia* are removed by flocculation/sedimentation and filtration, but are not readily inactivated by commonly employed drinking water disinfectants (*2*−*4*). EPA methods 1622 and 1623, the methods used in the United States for *C. parvum* and *G. lamblia* monitoring, are consistently plagued by poor recoveries. Furthermore, these methods include a number of steps that require high levels of analytical and biological expertise and are thus not readily done on-site. There has been a push for innovative approaches to pathogen detection to overcome the shortcomings of these monitoring strategies. Proposed techniques include PCR (*5*−*8*), antibody−antigen-based detection (*9*), and cell culture (*10*). Ideally, future methods will be capable of real time, multiplex detection and will have extremely low detection limits.

Raman scattering techniques have elicited significant interest for biomolecule detection as they provide several advantages over other spectroscopic techniques (*11*−*13*). Unlike IR and NMR, Raman signals are not affected by the presence of water, and Raman bands are much narrower than fluorescence bands. Raman-active molecules exhibit characteristic "fingerprint" spectra that can be used to definitively identify a molecule. Additionally, Raman responses are less susceptible to photobleaching than fluorescence responses, thus allowing longer signal collection times and improved signal averaging. Normal Raman signals are too weak to be of use in ultrasensitive detection methods, but surface-enhanced Raman spectroscopy (SERS) results in Raman signal enhancement factors as high as 10^{14} (*14*). SERS is the result of chemical and electromagnetic interactions between a roughened noble metal or noble metal nanoparticle and a surface-associated chemical (*15*). A resonance enhancement (surface-enhanced resonance Raman spectroscopy, SERRS) in addition to SERS enhancement can be observed when the target molecule has an electronic transition close to or coincident with the Raman excitation laser wavelength. SERS/SERRS has been used to study bacteria (*16*), for medical diagnostics (*17*), and for multiplex DNA and protein detection (*18, 19*). Despite a recent surge in SERS/SERRS-based biochemical detection, significantly less attention has been given to whole cell or microorganism detection.

Here we report on SERRS immunogold labeling for the detection of *C. parvum* and *G. lamblia*. The immunogold conjugates used in our study consist of gold nanoparticles conjugated with antibodies specific to *C. parvum* or *G. lamblia* and SERRS-active reporter molecules. This type of label has been used for SERS detection in a number of biomolecule detection studies (*20*−*25*). Unlike previous reports that have dealt with relatively small biomolecules such as proteins, viruses, and nucleic acids, we report here on the detection of protozoan pathogens in their infective, environmental form. With diameters between 3 and 13 μm, these organisms are large enough to be identified with an optical microscope when they have been fixed to glass microscope slides. We were therefore able to collect Raman maps across the surfaces of *C. parvum* cysts and *G. lamblia* oocysts, probing the interaction between the SERS-active immunogold and the organisms' surfaces. The Raman results elucidated the specificities and affinities of the immunogold conjugates to their respective analytes and allowed optimization of the immunogold synthesis procedure (i.e., antibody type, reporter dye identity, nanoparticle size). Our results suggest this type of detection strategy can be readily multiplexed to simultaneously detect numerous waterborne

* Corresponding author phone: (540) 231-3568; fax: (540) 231-7916; e-mail: pvikes@vt.edu

10.1021/es801531t CCC: $40.75
Published on Web 01/14/2009

pathogens. To our knowledge this is the first time living organisms have been labeled with immunogold and detected using $x-y$ Raman mapping.

Materials and Methods

Reagents and Buffer Solutions. $HAuCl_4 \cdot 3H_2O$, sodium citrate dehydrate (99+%), rhodamine B isothiocyanate (RBITC), fluorescein isothiocyanate (FITC), bovine serum albumin (BSA), and Tween 80 were purchased from Sigma-Aldrich (St. Louis, MO) and were used without further purification. Malachite green isothiocycante (MGITC) and X-rhodamine isothiocyanate (XRITC) were acquired from Invitrogen Corp. (Grand Island, NY). Mouse monoclonal IgG1 antibodies against *G. lamblia* and mouse polyclonal IgG antibodies against *G. lamblia* were obtained from Meridian Life Sciences (Cincinnati, OH). Mouse monoclonal IgM antibodies against *C. parvum* were obtained from Millipore. Antibodies (Temecula, CA) and mouse polyclonal IgG antibodies against *C. parvum* were purchased from Abcam Inc. (Cambridge, MA). IgG mouse polyclonal antibodies against *G. lamblia* were purchased from Meridian Life Sciences. Ultrapure water (>18 $M\Omega\ cm^{-1}$) was used in all aqueous solutions. The following buffers were used in the experiments: phosphate-buffered saline (PBS; 10 mM KH_2PO_4/Na_2HPO_4, 150 mM NaCl, 3 mM KCl, pH 7.4), borate buffer (BB; 2 mM, pH 9).

C. parvum oocysts and *G. lamblia* cysts were purchased from Waterborne, Inc. (New Orleans, LA). (Oo)cysts were washed twice by centrifugation and stored in a reagent water/0.1% Tween 80 solution at 4 °C. Washed (oo)cyst stocks were enumerated with a hemacytometer prior to use. Oocyst solutions were used within three months of purchase, and cysts were used within one month of purchase.

Instrumentation. Raman spectra were obtained with a JY Horiba LabRAM HR 800 spectrometer, with 600 grooves/mm gratings and a slit width of 150 μm. The instrument is equipped with an Olympus BX-41 petrographic microscope and an Ancor electronically cooled CCD detector. Excitation was provided by a 632.8 nm He−Ne laser. A long working distance 40× objective (NA = 0.75) was used to focus the laser beam. Sample slides were mounted on a motorized stage (Marzhauser EK-32), and an automated video camera was used to capture the optical image of the map area. For mapping experiments, Raman spectra from 1000 to 1800 cm^{-1} were collected at each map position with a 1 s acquisition. This spectral range was large enough to include several characteristic reporter molecule peaks and was small enough to prevent the 600 lines/mm grating from moving during collection. Transmission electron micrographs were collected with a JEOL 100 CX-II transmission electron microscope. UV−vis−NIR absorption spectra were obtained with a Varian Cary 5000 spectrophotometer.

Gold Nanoparticle and Immunogold Conjugate Syntheses. Gold nanoparticle seeds with diameters of 13 nm were prepared by the method of Frens (*26*). Gold nanoparticles with average diameters between 20 and 80 nm were prepared by a seeding method to obtain nanoparticle solutions with improved diameter homogeneities. Contaminants on glassware surfaces and particulates in the reagent solutions can act as nucleation sites for particle growth and can thus lead to nanoparticle solutions with large diameter dispersivities (*27*). For this reason, all glassware was bathed in aqua regia (75% HCl, 25% HNO_3) and rinsed copiously with ultrapure water prior to use and all reagent solutions were filtered through polycarbonate membrane filters with 0.2 μm pores prior to their use in nanoparticle synthesis. Immediately following nanoparticle synthesis, UV−vis absorption spectra were collected to measure the intrinsic surface plasmon peak whose position and width give information about nanoparticle size and homogeneity, respectively (*28*). If the surface plasmon peaks indicated the prepared nanoparticles were of the expected size and homogeneity, transmission electron microscopy (TEM) images were collected and were used in conjuncton with NIH ImageJ software to accurately quantify average nanoparticle diameters and particle homogeneity. Solutions that were found to have diameter dispersivities greater than 20% were discarded. Nanoparticle solutions were stored in amber glass bottles at 4 °C, and under these conditions the solutions were stable for several months.

Synthesis of the optimized *C. parvum* and *G. lamblia* immunogold conjugates was conducted by spiking 0.3 mL aliquots of 40 nm gold nanoparticles with 1.2 μL of methanolic RBITC and MGITC stock solutions (5 μM), respectively. The gold nanoparticles were allowed to react with the dye molecules overnight. The conjugates were centrifuged at 2000 rpm for 10 min, at which point the clear centrate containing unbound dye molecules was discarded and the loose sediment was resuspended in borate buffer. To the RBITC nanoparticle conjugates was added 3 μL of *C. parvum* IgM antibody concentrate, and to the MGITC nanoparticle conjugates was added 40 μL of *G. lamblia* IgG1 antibody concentrate. After reaction for 30 min, 30 μL of 10% BSA in borate buffer was added to each of the immunogold solutions to prevent immunogold loss during the following centrifugation steps. After reaction for another 90 min, the immunogold conjugates were centrifuged for 10 min at 2000 rpm. The centrate was discarded, and the loose sediment was resuspended in borate buffer. After a final centrifugation, the immunogold conjugates were resuspended in PBS buffer containing 0.1% Tween 80. The immunogold conjugates were filtered through polycarbonate membrane filters with 0.4 μm pores and stored at 4 °C for up to 48 h.

Protozoa were fixed by placing 20 μL drops containing 1000 oocysts and/or 1000 cysts into the wells of glass microscope slides. The slides were incubated with 5% BSA to discourage nonspecific immunogold binding. After unbound BSA was rinsed away, 50 μL of immunogold was added to the wells and the slides were placed in a humidity chamber for 30 min. The slides were rinsed in PBS buffer with 0.1% Tween 80 and dried, and then 50 μL of immunogold SERS label was pippetted onto the protozoa spots. The slides were incubated with immunogold in the humidity chamber for 2 h and then dried after being rinsed with PBS/0.1% Tween 80. A drop of 60% glycerol/40% PBS mounting media was placed over the wells, and a coverslip was sealed in place with adhesive. Finished slides were stored at 4 °C until analysis. Prior to the collection of Raman spectra, bright-field microscopy was used to locate organisms on the slide and to focus the Raman laser on an organism. *C. parvum* oocysts are spherical with average diameters of 3−5 μm, and *G. lamblia* are ovoid with long-axis diameters of approximately 11−14 μm and short-axis diameters of approximately 8−10 μm.

Results and Discussion

Gold Nanoparticle Production and Labeling. Small, organic molecules such as thiophenol, mercaptobenzoic acid, and napthalenethiol (*22, 24, 29*) are commonly used as reporter molecules in SERS immunogold as they can be readily conjugated to gold substrates. Resonance enhancement of the Raman signal, however, is not achieved with these molecules when visible excitation is employed. Resonance Raman can lead to an additional enhancement of the Raman signal and is desirable for low-level analyte detection. To address this, Doering and Nie labeled gold nanoparticles with fluorescent dye molecules containing isothiocyanate groups (*30*). In addition to binding strongly with gold through their isothiocyanate functional groups, these molecules have strong electronic transitions in the visible range. They are therefore capable of SERRS when visible excitation lasers are

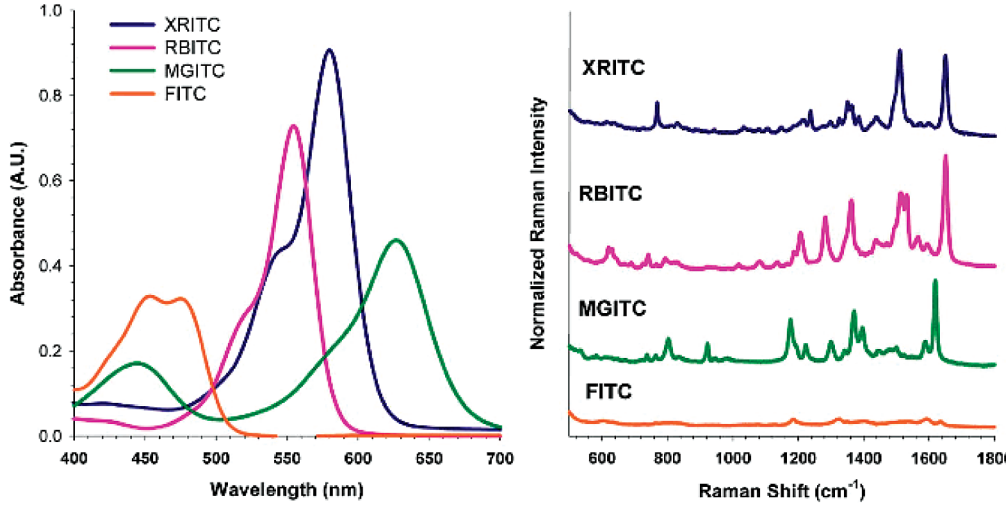

FIGURE 1. Absorption and SERRS spectra of fluorescent dyes: (left) absorption bands of XRITC, RBITC, MGITC, and FITC, (right) SERRS spectra of XRITC (20 nM), RBITC (20 nM), MGITC (50 nM), and FITC (50 nM) in the presence of 40 nm gold nanoparticles.

employed. We considered four fluorescent dye molecules with isothiocyanate functional groups for our *C. parvum* and *G. lamblia* immunogold conjugates: FITC, RBITC, MGITC, and XRITC. When added to the gold nanoparticle solutions, FITC Raman signals were much weaker than the signals of the other three molecules at the same dye concentration (Figure 1). FITC has an absorption maximum at 488 nm, while the other three molecules have maxima closer to the laser excitation wavelength of 633 nm (Figure 1), and thus, resonance Raman plays less of a role in the FITC signal enhancement. RBITC and XRITC exhibit very similar SERRS spectra, and the two dyes would be difficult to distinguish from one another in a multiplex Raman assay. MGITC and RBITC, however, have very different SERS spectra and thus enable simultaneous SERS detection of MGITC- and RBITC-conjugated immunogold. We employed MGITC and RBITC in the *G. lamblia* and the *C. parvum* immunogold conjugates, respectively. The MGITC− and RBITC−nanogold conjugates were prepared by spiking aliquots of nanogold with methanolic dye stocks, allowing the solution to react for several hours and then collecting the conjugates with centrifugation. Too much coverage by the dye molecule on the nanoparticles can lead to destabilized immunogold. As stable conjugate solutions are important for immunorecognition events, the appropriate dye concentrations for stable immunogold conjugates were established through dye stabilization assays (*22*) (see the Supporting Information for additional details).

Gold nanoparticles of 13 nm diameter prepared by citrate reduction of $HAuCl_4$ were initially used in this study because this size nanoparticle can be readily synthesized. Use of the 13 nm particles, however, led to poor SERRS enhancements of the RBITC and MGITC dye signals (Supporting Information, Figure S1). The SERS signals from immunogold prepared with the 13 nm particles could not be detected on the surface of oocysts and cysts incubated with their respective immunogold labels. Previous research has demonstrated that gold nanoparticles of ∼63 nm diameter are optimal for SERRS enhancement with 647 nm laser excitation (*31*). We therefore prepared gold nanoparticles with average diameters between 20 and 80 nm by seed-mediated growth (*27*) and compared the resulting SERS enhancements of RBITC solutions when excited with the 633 nm laser. Similar to previous reports, the Raman RBITC signals increased as the average diameter of the gold nanoparticles increased to about 60 nm (Supporting Information, Figure S2). TEM images of the solutions with particle diameters greater than 50 nm, however, showed irregularly shaped particles and often also contained unnucleated seed-sized particles. Furthermore, SERS enhancements of the >50 nm solutions were difficult to reproduce despite consecutive batches having similar average diameters. On the other hand, nanoparticle solutions prepared with average diameters below 50 nm were more spherical in shape, and SERS enhancements were highly reproducible. Although they exhibited lower enhancements than the 60 nm particles, they exhibited signals 100× greater than those of the 13 nm particles (Supporting Information, Figure S1). Nanoparticle solutions with average diameters of 38−42 nm could be repeatedly synthesized with standard deviations of less than 5 nm and were employed in all subsequent immunogold conjugate syntheses.

Gold nanoparticles with average diameters of 20, 40, 60, and 80 nm were also purchased from a common supplier (Ted Pella, Redding, CA). SERRS RBITC signals collected in the presence of these commercial nanoparticles were consistently lower than those collected with the nanoparticles prepared in our laboratory for each of these diameters. TEM analysis of the commercial and the synthesized nanoparticles indicated that although the solutions had particles with similar average diameters and dispersivities, the nanoparticles prepared in-house tended to be more faceted and ovoid in shape relative to the purchased nanoparticles (Supporting Information, Figure S3). Ellipsoidal gold nanoparticles and gold nanoparticles with sharp structural features have been shown to be better SERS enhancers than spherical gold nanoparticles in previous work (*32*).

Immunogold Optimization. Immunogold labels were prepared for *C. parvum* and *G. lamblia* with both polyclonal and monoclonal antibodies. For *C. parvum*, an IgM antibody immunogold and a polyclonal IgG fraction antibody immunogold were prepared. For *G. lamblia*, an IgG1 antibody immunogold and a polyclonal IgG fraction immunogold were prepared. Past papers describing the synthesis of immunogold for SERS detection have recommended that antibody concentrations that are 150% of the concentration needed to coat the particle surface, as determined by flocculation tests (*33, 34*), should be employed to maximize particle stability (*21, 22*). We therefore performed flocculation tests for each of our commercial antibodies to determine the amount required to coat the nanoparticle surfaces. The commercial *C. parvum* and *G. lamblia* polyclonal IgG antibodies saturated the 40 nm particle−dye molecule conjugates when the antibody concentrations were >8 μg/mL, and thus, 12 μg/mL was used in subsequent polyclonal immunogold syntheses. *C. parvum* IgM monoclonal antibodies saturated the surface of the 40 nm gold nanoparticles when >6 μL of the monoclonal IgM solution (the exact ascites

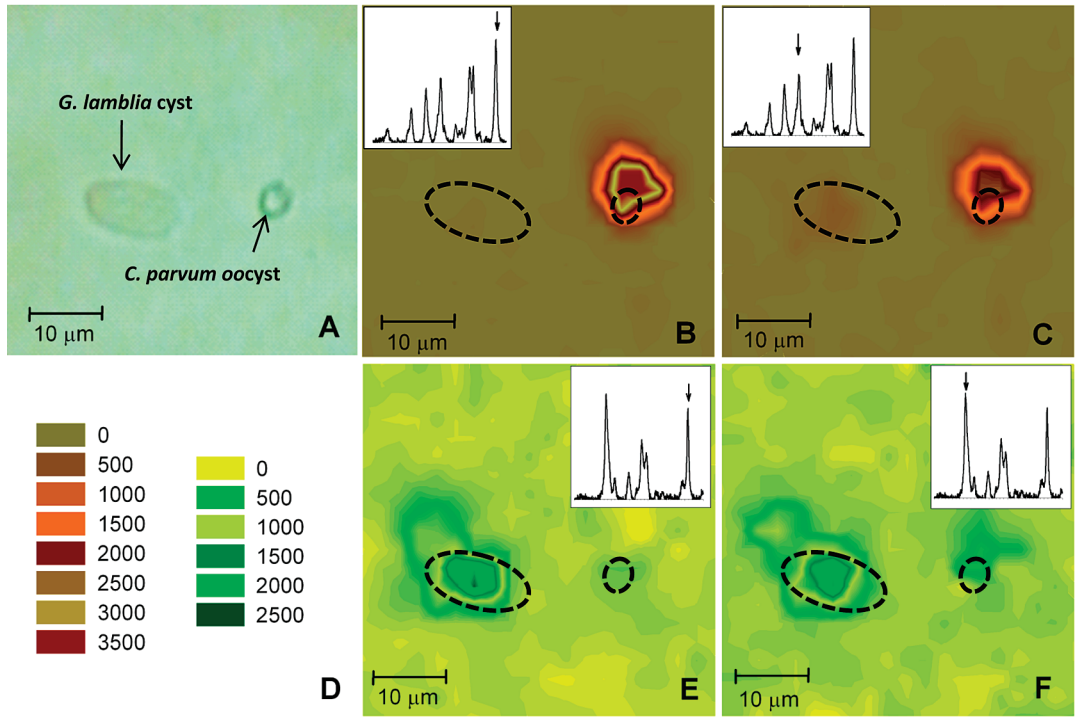

FIGURE 2. Raman *x*−*y* maps of a *G. lamblia* cyst and a *C. parvum* oocyst. Dashed lines represent outlines of the organism location. Raman mapping settings: 20 × 20 measurements (400 total), 2 μm steps, 1 s acquisition time. (A) Optical microscope image of a cyst and an oocyst. (B) Raman map of the 1647 cm^{-1} RBITC peak. Inset: RBITC SERRS spectrum with the arrow identifying the 1647 cm^{-1} peak. (C) Raman map of the 1360 cm^{-1} RBITC peak. Inset: RBITC SERRS spectrum with the arrow identifying the 1360 cm^{-1} peak. (D) Raman intensity key. (E) Raman map of the 1618 cm^{-1} MGITC peak. Inset: MGITC SERRS spectrum with the arrow identifying the 1618 cm^{-1} peak. (F) Raman map of the 1175 cm^{-1} MGITC peak. Inset: MGITC SERRS spectrum with the arrow identifying the 1175 cm^{-1} peak.

IgM concentration was not provided by the supplier) was added to 1 mL of nanoparticle solution, so 9 μL of the antibody concentrate was used per milliliter of nanoparticles in subsequent syntheses. Interestingly, the addition of the *G. lamblia* and *C. parvum* IgG1 monoclonal antibodies led to destabilized nanoparticle solutions at all tested antibody concentrations, and thus, it was impossible to find an appropriate IgG1 concentration with flocculation tests. We did, however, find that adding BSA to the nanoparticle−antibody conjugates after they had reacted for 20 min resulted in a stabilized immunogold solution. In subsequent IgG1 antibody immunogold syntheses, we used the concentration of antibodies determined to be adequate in the polyclonal IgG flocculation assays (12 μg/mL) and included this BSA stabilization step.

The monoclonal immunogold and the polyclonal immunogold solutions were incubated with their respective organisms, and their binding characteristics were compared. Raman measurements were collected at three points across the surface of the oocysts and six points along the cyst surfaces, and the collected peak intensities were averaged for each type of immunogold. Raman signals collected on *Giardia* cysts incubated with monoclonal *Giardia* IgG1 immunogold resulted in positive label signals on 20 out of 20 cysts, while cysts incubated with polyclonal *Giardia* immunogold resulted in positive signals on 18 of 20 cysts. On average, the immunogold SERS signals were an order of magnitude higher for the monoclonal *Giardia* IgG1 immunogold labeled cysts than for the polyclonal *Giardia* immunogold labeled cysts. For *C. parvum* immunogold, 20 out of 20 oocysts resulted in positive signals when incubated with the *C. parvum* IgM monoclonal antibody immunogold and 18 out of 20 oocysts had positive signals when incubated with *C. parvum* polyclonal antibody immunogold. The average signal intensities were approximately 20% higher on the oocysts incubated with monoclonal *C. parvum* IgM antibody immunogold. Maps collected across oocysts and cysts incubated with the two polyclonal immunogolds showed inconsistent coverage of the labels, while maps collected across oocysts and cysts incubated with the monoclonal immunogolds showed full coverage of the immunogold signals. Specification sheets provided by the antibody vendors indicated that the monoclonal antibodies were specific to surface antigens on the oocysts and cysts. The polyclonal IgG antibodies to *C. parvum* and *G. lambia* were probably less successful in SERS detection because they consist of a mixture of antibodies specific to different oocyst and cyst antigens. On the basis of these results, it was determined that the monoclonal antibodies were better suited for SERS immunogold labeling. Subsequently, immunogold was prepared only with monoclonal antibodies.

The selectivity and sensitivity of the monoclonal immunogold solutions to their respective organisms were determined by examining 20 oocysts and 20 cysts for the characteristic MGITC and RBITC signals after incubation with both anti-*Giardia* and anti-*C. parvum* monoclonal immunogold solutions. Raman measurements were collected at three points across the surface of an oocyst and six points along the surface of a cyst. An RBITC signal was considered a true positive if it was colocated with *C. parvum*, and an MGITC signal was considered a true positive if it was colocated with *G. lamblia*. Signals were considered false positives if they were obtained on the incorrect organism. *Cryptosporidium* immunogold showed a specificity of 85% and a sensitivity of 100%. The specificity of the *Giardia* immunogold was 100% and the sensitivity was 100%.

As illustrated in Figure 2A,B, a map of the intensity of the characteristic Raman RBITC peak at 1647 cm^{-1} shows the location of a *Cryptosporidium parvum* oocyst. A map of the characteristic RBITC peak at 1360 cm^{-1} gives similar results

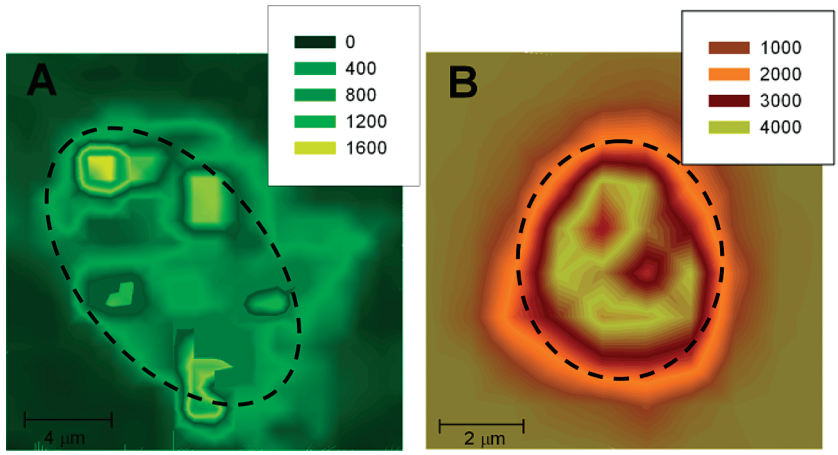

FIGURE 3. Raman *x*−*y* maps of a *G. lamblia* cyst (A) and a *C. parvum* oocyst (B). The dashed line represents the outline of the organism as determined with optical microscopy. (A) Intensity of the 1618 cm^{-1} MGITC peak on the surface of a *Giardia* cyst. Mapping settings: 20 × 20 map with 1 μm steps, 1 s acquisition time. (B) Intensity of the 1645 cm^{-1} RBITC peak across the surface of a *C. parvum* oocyst. Mapping settings: 10 × 10 map with 1 μm steps, 1 s acquisition time.

(Figure 2C). The area on the Raman map exhibiting an RBITC signal has a diameter of approximately 10 μm, and this is approximately twice the size of the oocyst. The 40× objective has a nominal spot size of ~1 μm, and a step size of 2 μm was used to collect the data presented in Figure 2. As a result, the RBITC signal is detected over a larger area than the actual area of the organism. Similarly, the characteristic MGITC peaks at 1618 and 1175 cm^{-1} were observed across the *G. lamblia* surface (Figure 2E,F). As expected on the basis of the sensitivity and specificity determinations, there were no MGITC signals observed across the surface of the *C. parvum* oocysts and only rarely was an RBITC signal observed at any point on the surface of the *Giardia* cysts. This result indicates that the respective antibodies of the two protozoa do not cross-react. It also suggests that the RBITC and MGITC dyes in the immunogold conjugates do not swap between one type of immunogold and another during incubation.

Raman maps of the intensities of the RBITC 1647 cm^{-1} peak (Figures 2B) and the MGITC 1618 cm^{-1} peak (Figures 2E) correctly differentiate between oocysts and cysts. This type of simplistic characteristic peak identification, however, may lead to the misidentification of organisms. For example, upon close inspection of the map in Figure 2C, one can see that there is a slight detection of the RBITC 1360 cm^{-1} peak over the area of the *Giardia* cyst. Similarly in Figure 2F, it appears that the MGITC 1175 cm^{-1} peak is detected over the surface of the *C. parvum* oocyst. This occurs due to an interfering peak in the MGITC SERRS spectrum at 1365 cm^{-1} that is detected in the 1360 cm^{-1} map (Figure 2F) and an interfering peak in the RBITC SERRS spectrum at 1200 cm^{-1} that is detected in the 1175 cm^{-1} map (Figure 2C). This type of interference demonstrates the need to use entire spectra to correctly identify immunogold labels in multiplex detection rather than only one or two characteristic peaks. This requirement will become increasingly important as additional organism−immunogold pairs are added to the technique and when real drinking water samples are analyzed.

Small SERRS maps were collected across the surfaces of oocysts and cysts with 1 μm increment steps to better characterize immunogold label distribution (Figure 3). In Figure 3A, the MGITC 1618 cm^{-1} signal is sporadic with localized hot spots on the cyst surface. The RBITC 1647 cm^{-1} signal intensity in Figure 3B, however, is more consistent across the surface of the oocyst. Average RBITC intensities on the oocyst surfaces were ~1.5−2 times larger than the intensities of the MGITC signals on the *Giardia* cysts. Raman measurements of MGITC and RBITC dyes in 40 nm nanoparticle solutions showed similar differences in signal intensities (Figure 1). When anti-*Giardia* immunogold was prepared with RBITC instead of MGITC and incubated with *Giardia*, the RBITC Raman signals were consistently measured across the *Giardia* cysts and were as high as those observed when *C. parvum* oocysts were incubated with RBITC anti-*C. parvum* immunogold. Therefore, it was determined that the sporadic coverage and weaker MGITC signals across the *Giardia* cysts were due mostly to the weaker MGITC signal instead of being the result of differences in the binding affinities of the two types of antibodies to their respective organisms.

A major problem with the current EPA pathogen detection methods is the length of time it takes laboratories to perform the analyses. Thus, the proposed SERS-based method would be a major improvement to these methods if it is capable of providing rapid results. Accordingly, a Raman mapping method to detect reporter immunogold bound to pathogens will require the careful selection of appropriate step sizes. Larger steps allow greater areas to be scanned in less time, but can skip over organisms, whereas small step sizes clearly outline organisms but require longer collection times. For *C. parvum* oocyst detection with a 40× objective, a step size of 7 μm was capable of detecting most oocysts (Supporting Information, Figure S4), but a step size of 10 μm "missed" many oocysts. The 43 × 43 Raman map shown in Figure S4 with 7 μm steps scans an area of about 0.3 mm^2. With a 1 s acquisition time, a map this size took approximately 1 h to collect. Raman spectrometers are now available with rapid scanning capabilities, however, and the mapping acquisitions with these instruments cover much larger areas in much less time. It may be necessary in future methods to quickly scan large areas with large steps (7 μm) and then zoom in on the map areas that have demonstrated positive hits. If the zoomed-in map with small steps produces a map of the label corresponding to the size and shape of the organism, a positive result would be recorded.

We have reported here on work toward the development of an SERRS-based detection technique for *C. parvum* and *G. lamblia*. This work is especially promising as there are numerous Raman-active molecules available that are capable of being incorporated into immunogold labels that can detect a number of waterborne pathogens simultaneously. Because it depends on spectral recognition instead of fluorescence microscopy, this type of detection can be incorporated into a fully automated monitoring strategy. Our laboratory is currently working on the synthesis of a filter capable of collecting and concentrating waterborne pathogens that will be coupled with SERRS-based detection. Additional work

will be needed prior to incorporation of the proposed SERRS technique into a commercial pathogen detection method. This work will need to address the shelf life of the immunogold conjugates and will need to determine the reproducibility and detection limits of the SERS detection method when combined with a concentration technique. Additionally, the effect of real water will need to be assessed as varied water chemistries and the presence of extraneous debris may affect the binding efficiencies of the immunogold labels.

Acknowledgments

This work was supported by a National Science Foundation Graduate Student Fellowship, a Waste Policy Institute Fellowship, and an AdvanceVT doctoral fellowship to K.L.R. and through a research grant from the National Science Foundation (BES-0606995). We thank Charles Farley and Steve McCartney for their help with the Raman and TEM instrumentation.

Supporting Information Available

Materials and methods and supporting figures. This material is available free of charge via the Internet at http://pubs.acs.org.

Literature Cited

(1) Bacterial standard for drinking water. *Public Health Report*; U.S. Treasury Department: Washington, DC, 1914; Vol. 29, pp 2959−2966.

(2) Korich, D. G.; Mead, J. R.; Madore, M. S.; Sinclair, N. A.; Sterling, C. R. Effects of ozone, chlorine dioxide, chlorine, and monochloramine on *Cryptosporidium-parvum* oocyst viability. *Appl. Environ. Microbiol.* **1990**, *56* (5), 1423–1428.

(3) Venczel, L. V.; Arrowood, M.; Hurd, M.; Sobsey, M. D. Inactivation of *Cryptosporidium parvum* oocysts and *Clostridium perfringens* spores by a mixed-oxidant disinfectant and by free chlorine. *Appl. Environ. Microbiol.* **1997**, *63* (4), 1598–1601.

(4) Betancourt, W. Q.; Rose, J. B. Drinking water treatment processes for removal of *Cryptosporidium* and *Giardia*. *Vet. Parasitol.* **2004**, *126* (1−2), 219–234.

(5) Deng, M. Q.; Cliver, D. O.; Mariam, T. W. Immunomagnetic capture PCR to detect viable *Cryptosporidium parvum* oocysts from environmental samples. *Appl. Environ. Microbiol.* **1997**, *63* (8), 3134–3138.

(6) Fontaine, M.; Guillot, E. An immunomagnetic separation-real-time PCR method for quantification of *Cryptosporidium parvum* in water samples. *J. Microbiol. Methods* **2003**, *54*, 29–36.

(7) Xiao, L.; Singh, A.; Limor, J.; Graczyk, T. K.; Gradus, S.; Lal, A. Molecular characterization of *Cryptosporidium* oocysts in samples of raw surface water and wastewater. *Appl. Environ. Microbiol.* **2001**, *67* (3), 1097–1101.

(8) Di Giovanni, G. D.; Hashemi, F. H.; Shaw, N. J.; Abrams, F. A.; LeChevallier, M. W.; Abbaszadegan, M. Detection of infectious *Cryptosporidium parvum* oocysts in surface and filter backwash water samples by immunomagnetic separation and integrated cell culture-PCR. *Appl. Environ. Microbiol.* **1999**, *65* (8), 3427–3432.

(9) Kalele, S. A.; Kundu, A. A.; Gosavi, S. W.; Deobagkar, D. N.; Deobagkar, D. D.; Kulkarni, S. K. Rapid detection of *Escherichia coli* by using anti body-conjugated silver nanoshells. *Small* **2006**, *2* (3), 335–338.

(10) LeChevallier, M. W.; Giovanni, G. D. D.; Clancy, J. L.; Bukhari, Z.; Bukhari, S.; Rosen, J. S.; Sobrinho, J.; Frey, M. M. Comparison of method 1623 and cell culture-PCR for detection of *Cryptosporidium* spp. in source waters. *Appl. Environ. Microbiol.* **2003**, *69* (2), 971–979.

(11) Vo-Dinh, T.; Stokes, D. L.; Griffin, G. D.; Volkan, M.; Kim, U. J.; Simon, M. I. Surface-enhanced Raman scattering (SERS) method and instrumentation for genomics and biomedical analysis. *J. Raman Spectrosc.* **1999**, *30* (9), 785–793.

(12) Kneipp, K.; Kneipp, H.; Itzkan, I.; Dasari, R. R.; Feld, M. S. Ultrasensitive chemical analysis by Raman spectroscopy. *Chem. Rev.* **1999**, *99* (10), 2957–2976.

(13) Gessner, R.; Rosch, P.; Petry, R.; Schmitt, M.; Strehle, M. A.; Kiefer, W.; Popp, J. The application of a SERS fiber probe for the investigation of sensitive biological samples. *Analyst* **2004**, *129* (12), 1193–1199.

(14) Kneipp, K.; Wang, Y.; Kneipp, H.; Perelman, L. T.; Itzkan, I.; Dasari, R.; Feld, M. S. Single molecule detection using surface-enhanced Raman scattering (SERS). *Phys. Rev. Lett.* **1997**, *78* (9), 1667–1670.

(15) Haynes, C. L.; McFarland, A. D.; Van Duyne, R. P. Surface-enhanced Raman spectroscopy. *Anal. Chem.* **2005**, *77* (17), 338A–346A.

(16) Premasiri, W. R.; Moir, D. T.; Klempner, M. S.; Krieger, N.; Jones, G.; Ziegler, L. D. Characterization of the surface enhanced Raman scattering (SERS) of bacteria. *J. Phys. Chem. B* **2005**, *109* (1), 312–320.

(17) Allain, L. R.; Vo-Dinh, T. Surface-enhanced Raman scattering detection of the breast cancer susceptibility gene BRCA1 using a silver-coated microarray platform. *Anal. Chim. Acta* **2002**, *469* (1), 149–154.

(18) Cao, Y. W. C.; Jin, R. C.; Mirkin, C. A. Nanoparticles with Raman spectroscopic fingerprints for DNA and RNA detection. *Science* **2002**, *297* (5586), 1536–1540.

(19) Jin, R. C.; Cao, Y. C.; Thaxton, C. S.; Mirkin, C. A. Glass-bead-based parallel detection of DNA using composite Raman labels. *Small* **2006**, *2* (3), 375–380.

(20) Driskell, J. D.; Kwarta, K. M.; Lipert, R. J.; Porter, M. D.; Neill, J. D.; Ridpath, J. F. Low-level detection of viral pathogens by a surface-enhanced Raman scattering based immunoassay. *Anal. Chem.* **2005**, *77* (19), 6147–6154.

(21) Cui, Y.; Ren, B.; Yao, J. L.; Gu, R. A.; Tian, Z. Q. Synthesis of $Ag_{core}Au_{shell}$ bimetallic nanoparticles for immunoassay based on surface-enhanced Raman spectroscopy. *J. Phys. Chem. B* **2006**, *110* (9), 4002–4006.

(22) Xu, S. P.; Ji, X. H.; Xu, W. Q.; Li, X. L.; Wang, L. Y.; Bai, Y. B.; Zhao, B.; Ozaki, Y. Immunoassay using probe-labelling immunogold nanoparticles with silver staining enhancement via surface-enhanced Raman scattering. *Analyst* **2004**, *129* (1), 63–68.

(23) Grubisha, D. S.; Lipert, R. J.; Park, H. Y.; Driskell, J.; Porter, M. D. Femtomolar detection of prostate-specific antigen: An immunoassay based on surface-enhanced Raman scattering and immunogold labels. *Anal. Chem.* **2003**, *75* (21), 5936–5943.

(24) Ni, J.; Lipert, R. J.; Dawson, G. B.; Porter, M. D. Immunoassay readout method using extrinsic Raman labels adsorbed on immunogold colloids. *Anal. Chem.* **1999**, *71*, 4903–4908.

(25) Su, X.; Zhang, J.; Sun, L.; Koo, T. W.; Chan, S.; Sundararajan, N.; Yamakawa, M.; Berlin, A. A. Composite organic-inorganic nanoparticles (COINs) with chemically encoded optical signatures. *Nano Lett.* **2005**, *5* (1), 49–54.

(26) Frens, G. Controlled nucleation for the regulation of the particle size in monodisperse gold suspensions. *Nat. Phys. Sci.* **1973**, *241*, 20–22.

(27) Brown, K. R.; Walter, D. G.; Natan, M. J. Seeding of colloidal Au nanoparticle solutions. 2. Improved control of particle size and shape. *Chem. Mater.* **2000**, *12* (2), 306–313.

(28) Keating, C. D.; Musick, M. D.; Keefe, M. H.; Natan, M. J. Kinetics and thermodynamics of Au colloid monolayer self-assembly. *J. Chem. Educ.* **1999**, *76* (7), 949–955.

(29) Mulvaney, S. P.; Musick, M. D.; Keating, C.; Natan, M. J. Glass-coated, analyte-tagged nanoparticles: A new tagging system based on detection with surface-enhanced Raman scattering. *Langmuir* **2003**, *19*, 4784–4790.

(30) Doering, W. E.; Nie, S. Spectroscopic tags using dye-embedded nanoparticles and surface-enhanced Raman scattering. *Anal. Chem.* **2003**, *75* (22), 6171–6176.

(31) Krug, J. T.; Wang, G. D.; Emory, S. R.; Nie, S. M. Efficient Raman enhancement and intermittent light emission observed in single gold nanocrystals. *J. Am. Chem. Soc.* **1999**, *121* (39), 9208–9214.

(32) Orendorff, C. J.; Gole, A.; Sau, T. K.; Murphy, C. J. Surface-enhanced Raman spectroscopy of self-assembled monolayers: Sandwich architecture and nanoparticle shape dependence. *Anal. Chem.* **2005**, *77* (10), 3261–3266.

(33) Hayat, M. A. *Colloidal Gold*; Academic Press, Inc.: San Diego, CA, 1989; Vols. *1*−*3*.

(34) Ni, J.; Lipert, R. J.; Dawson, G. B.; Porter, M. D. Immunoassay readout method using extrinsic Raman labels adsorbed on immunogold colloids. *Anal. Chem.* **1999**, *71* (21), 4903–4908.

ES801531T